Mon. Not. R. Astron. Soc. **264,** 16–34 (1993)

ROSAT studies of the composition and structure of DA white dwarf atmospheres

M. A. Barstow,[1] T. A. Fleming,[2] C. J. Diamond,[3] D. S. Finley,[4] A. E. Sansom,[1]★ S. R. Rosen,[1] D. Koester,[5] M. C. Marsh,[1] J. B. Holberg[6] and K. Kidder[6]

[1] *Department of Physics and Astronomy, University of Leicester, University Road, Leicester LE1 7RH*
[2] *Max Planck Institut für Extraterrestriche Physik, Giessenbachstrasse, D-8046 Garching bei München, Germany*
[3] *School of Physics and Space Research, University of Birmingham, Edgbaston, Birmingham B15 2TT*
[4] *Center for EUV Astrophysics, University of California, Berkeley, CA 94720, USA*
[5] *Department of Physics and Astronomy, Louisiana State University, Baton Rouge, LA 70803-4001, USA*
[6] *Lunar and Planetary Laboratory, Space Science Building, University of Arizona, Tucson, AZ 85721, USA*

Accepted 1993 February 16. Received 1993 February 7; in original form 1992 October 19

ABSTRACT

We present here a detailed study of a sample of hot DA white dwarfs detected in the EUV and soft X-ray bands by *ROSAT* during its all-sky survey. The survey data are combined with additional *ROSAT* pointed-phase observations, earlier *EXOSAT* results and the available optically determined effective temperatures and gravities. We show that the spectra of those stars with temperatures below ≈40 000 K are well described by nearly pure H atmospheres, with only very small traces of additional opacity due to He allowed by the data. Above ≈40 000 K, however, neither homogeneous nor stratified H + He models can, in general, explain the observed EUV and X-ray fluxes. We conclude that additional sources of opacity in the form of trace metals must be present in the photospheres of these stars. The disappearance of this material when the stars cool below 40 000–50 000 K is in agreement with theoretical radiative levitation calculations. We propose that these results are direct observational evidence that the composition of most DA white dwarf atmospheres is dominated by the balance between gravitational and radiative forces. Limits on the H-layer mass obtained for the cooler stars indicate that He makes only a minimal, if any, contribution to the EUV/soft X-ray opacity in the phosphere.

Key words: stars: atmospheres – white dwarfs – ultraviolet: stars – X-rays: stars.

1 INTRODUCTION

A major outstanding problem in the study of white dwarfs is their division into two distinct categories, having either hydrogen-rich or helium-dominated atmospheres, and the routes by which they evolve from possible progenitors (see e.g. Sion 1986 and Weidemann 1990 for reviews). Studies of the white dwarf luminosity function show that, in the temperature range 40 000–80 000 K, the H-rich DA white dwarfs outnumber the He-rich DOs by a factor of 7 (Fleming, Liebert & Green 1986), whereas H-rich planetary nebula central stars, the most likely progenitors of DAs, are no more numerous than He-rich examples. Another difficulty is the apparent absence of He-rich stars in the temperature range 30 000–45 000 K, providing a break between the hot DO and cooler DB white dwarfs on the cooling sequence. In the absence of demonstrated selection effects, the existence of this 'DB gap' provides strong support for the hypothesis that the H- and He-dominated stars are not distinct evolutionary sequences, and that DOs can evolve into DAs and at least some DAs can evolve into DBs. Several physical processes can be invoked as possible explanations of what is seen. White dwarfs have strong gravitational fields and, in the absence of any competing effect, He and heavier elements will tend to sink out of an atmosphere, leaving a layer of H at the top. DAs might therefore be formed from DOs through the build-up of thin ($<10^{-8}M_{\odot}$) H layers through gravitational settling of He. DBs then appear with the onset of convection at ≈30 000 K, which mixes the thin H layer back into the He envelope. However, this is in

★Present address: Department of Physics and Astronomy, University of Central Lancashire, Preston PR1 2TQ.

conflict with evolutionary calculations which predict that DA white dwarfs should be formed with massive H layers ($\approx 10^{-4}$ $M_\odot$, e.g. Iben & Tutukov 1984; Iben & MacDonald 1985; Koester & Schönberner 1986). Gravitational stratification may be slowed down or stopped by radiation pressure. For example, Morvan, Vauclair & Vauclair (1986), Chayer, Fontaine & Wesemael (1989) and Vauclair (1989) have shown theoretically that C, N and Si can be supported in DA atmospheres at temperatures above $\approx 40\,000$ K. However, radiative levitation is not able to support He below the $\approx 65\,000$ K upper limit of the DA temperature range (Vennes et al. 1988). Other processes that can affect the photospheric composition are accretion of material from the interstellar medium or convective mixing, which dredges up those species that have already settled out under the influence of gravity. Detailed calculations rule out accretion as a viable mechanism to explain the observed properties of hot DA stars (Vennes et al. 1988).

A thorough understanding of the compositional evolution of white dwarfs requires measurements of the abundances of trace elements. It has been demonstrated, from observations made with the *EXOSAT* and *Einstein* satellites, that the emergent extreme-UV (EUV) and X-ray fluxes from hot DA white dwarfs are very sensitive to the presence of trace elements (notably He and possibly heavier elements) in their atmospheres (Paerels & Heise 1989). If the temperature of a particular star is known, EUV/soft X-ray data can be used to estimate the abundance of He in the envelope, making the assumption that it is homogeneously mixed. From a sample of around 20 DA white dwarfs, Paerels & Heise (1989) found weak evidence for a trend of increasing He abundance with increasing effective temperature. An alternative, and probably more physically realistic, interpretation of the data assumes that the atmosphere has a stratified structure with a thin layer of H overlying a predominantly He atmosphere. In this situation, the free parameter is the mass of the H layer (M_H) overlying trace amounts of He which have diffused across the H/He boundary. A study by Koester (1989) found no strong correlation between M_H and T_{eff} other than a general tendency for thinner H layers to occur in hotter stars. All of the work discussed above makes the implicit assumption that He is the only significant opacity source in the EUV/X-ray region. This is not necessarily true. The *EXOSAT* grating spectrum of the DA white dwarf Feige 24 cannot be explained by either homogeneous or stratified models (Paerels et al. 1986; Vennes et al. 1989). Vennes et al. (1989), however, showed that a photospheric model with trace metals can fit the observations. More recently, we have studied the hot DA white dwarf G191−B2B, with a combination of *ROSAT* and *EXOSAT* data, high signal-to-noise ratio optical spectra and a new determination of the interstellar H I along the line of sight (Barstow et al. 1993a). Again, simple H + He models are not able to explain all of the observations, and it is clear that additional EUV/X-ray opacity is present in the atmosphere of the star. This is confirmed by a recent EUV spectrum obtained with a rocket-borne instrument, which shows no sign of the He II 228-Å edge, but does show absorption features thought to result from O III and Fe VI (Wilkinson, Green & Cash 1992).

So far, there is insufficient evidence to decide which physical model, or combination of models, is the correct representation of DA white dwarf photospheres. The *ROSAT* all-sky EUV and X-ray surveys present us with an opportunity to resolve the issue. Primarily, there is a much larger sample of objects to study, improving the statistical basis of any composition/T_{eff} correlation. Secondly, the photometric bands available yield improved spectral resolution over earlier instruments. We present here a detailed analysis of a sample of DA white dwarfs detected in the *ROSAT* surveys and for which we already have good determinations of T_{eff} and surface gravity from analysis of the optical Balmer line profiles. Where available, we also include data from *ROSAT* pointed-phase or earlier *EXOSAT* observations.

2 THE *ROSAT* ALL-SKY SURVEY AND POINTED OBSERVATIONS

2.1 *ROSAT* instruments and survey strategy

ROSAT has two co-aligned imaging instruments. These have been described in detail elsewhere, but those details that are relevant to the discussion are briefly reiterated here. The X-ray telescope has a positional sensitive proportional counter (PSPC) at the focal plane and covers the energy range ≈ 0.1–2.4 keV (5.2–100 Å: Pfefferman et al. 1986). Although the PSPC has modest energy resolution, which we will exploit in the future, in this study we use just the integrated count rate in the band between ≈ 0.1 and 0.4 keV (25–100 Å). During the pointed phase of the mission, the PSPC can also be used in conjunction with a boron filter. The combined effects of the boron edge at 0.18 keV (67.6 Å) and the more rapidly decreasing instrumental effective area towards lower energies effectively subdivides the PSPC band, providing two essentially independent points with which to constrain the white dwarf energy distribution. The EUV waveband is covered by the Wide Field Camera (WFC: Wells et al. 1990). For survey observations, two broad-band filters were employed: S1, covering the energy range 90–200 eV (60–140 Å), and S2, covering the band 60–110 eV (112–200 Å). Two additional filters are available for the pointed phase of the mission, extending the coverage to lower energies: P1 spans 56–83 eV (150–220 Å) and P2 spans 17–24 eV (500–730 Å). Fig. 1 shows the effective areas of the *ROSAT* PSPC, S1, S2 and P1 bands (no P2 data are available for the stars in our sample) and compares them with the responses of the prime *EXOSAT* thin lexan (3Lx) and aluminium/parylene (AlP) filters. It can be seen that the *ROSAT* instruments yield about a factor of 3 better spectral resolution than available with *EXOSAT*.

The *ROSAT* soft X-ray and EUV all-sky survey was conducted from 1990 July to 1991 January. During each *ROSAT* orbit, the instruments scanned a great circle on the sky on a path passing through the ecliptic poles. In order to maintain alignment of the solar panels with the Sun, the ecliptic longitudes observed drifted by $\approx 1°$ per day. In this fashion, the whole sky was covered in 6 months. Data from the two instruments were processed independently. PSPC images were divided into strips of ecliptic longitude, whereas those of the WFC were divided into $2° \times 2°$ 'smallmaps' once the full survey exposure had been achieved for a given region of sky. In both cases, the data were searched for point sources and the measured positions were compared with catalogues of known objects.

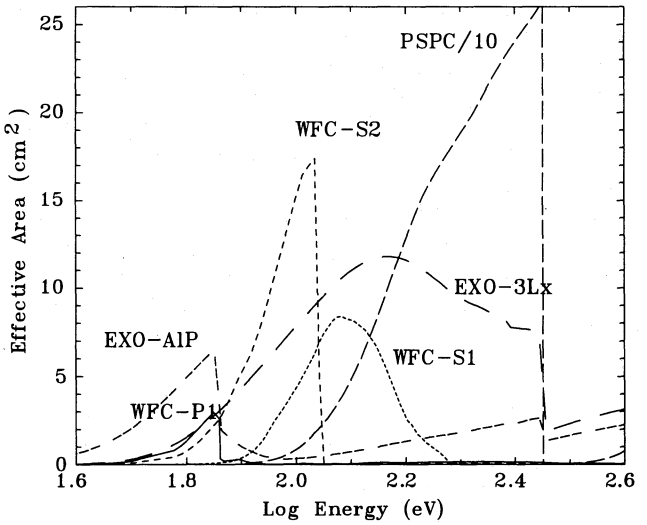

Figure 1. Effective area as a function of photon energy for the *ROSAT* PSPC, with WFC S1, S2 and P1 filters, and the *EXOSAT* thin lexan and aluminium/parylene filters.

2.2 Known white dwarfs detected in the *ROSAT* survey

A catalogue of 384 EUV sources, selected with very stringent criteria, has recently been published (Pounds et al. 1993). A total of 55 objects from this catalogue are known hot white dwarfs and a similar number are new discoveries. An estimate of the total number of known white dwarfs with temperatures exceeding 20 000 K (*ROSAT* is virtually insensitive to stars with temperatures below this value) suggests that ≈ 500 known stars should have been detected by the survey (Fleming et al. 1993). The fact that we see only 10 per cent of the objects we might expect is a surprise. We are unable to explain this result by the effects of interstellar absorption (see Fleming et al. 1993). For example, it has been predicted (Barstow 1989) that approximately twice as many DA white dwarfs should be detected by the PSPC compared to the WFC. However, the observed ratio of PSPC to WFC detections of DA stars is around 1:1. If H I columns were greater than expected, the number of WFC detections would tend to *decrease* with respect to those of the PSPC. Conversely, lower than anticipated H I densities could increase the relative numbers of stars in the WFC data, but this is not consistent with the obvious shortfall of detections from the known white dwarf catalogues. Predictions of the ratio of white dwarfs detected with the PSPC and WFC make simplistic assumptions regarding the expected composition of their atmospheres. Previous calculations (Barstow 1989) assumed a canonical He:H ratio of 10^{-4} in a homogeneous mixture. The apparent shortfall of PSPC detections is strong circumstantial evidence for the presence of additional opacity in DA white dwarf atmospheres.

2.3 The sample of DA white dwarfs selected from the survey

Studies of DA white dwarf atmospheres with EUV/X-ray photometric observations require that five main parameters be determined: $T_{\rm eff}$, log g, H I column ($N_{\rm H}$), He abundance (or $M_{\rm H}$ for a stratified model) and a normalization constant. The emergent fluxes depend only weakly on log g over the range of values covered by DA white dwarfs, but the remaining parameters have a large effect on the observed count rates. It is possible to fix log g at some canonical value (usually log $g = 8.0$) in the absence of any other information, but a minimum of four independent photometric observations are required to determine the other parameters. Often only two or three are available. The usefulness of the EUV/X-ray data can be maximized if one parameter is already known. For example, Paerels & Heise (1989) fixed the value of $T_{\rm eff}$ in their modelling, from various optical or UV determinations, which then allowed the EUV/X-ray data to constrain the He abundance. One important limitation in their work lies in the disparate nature of, and the relative uncertainties in, their $T_{\rm eff}$ measurements. In particular, systematic differences between temperatures estimated by different methods may have a significant effect on the abundances implied by the EUV/X-ray data. While the possible impact of systematic differences in $T_{\rm eff}$ is difficult to evaluate in the Paerels & Heise study, the important limitation imposed by the large uncertainties in $T_{\rm eff}$ is readily apparent.

Recently, several systematic surveys of $T_{\rm eff}$ and log g have been made for substantial samples of DA white dwarfs using the common technique of fitting synthetic line profiles to the observed Balmer lines and, where available, Lyman α. Two studies, of particular importance to the observations reported here, are those of Kidder (1991) and Finley, Koester & Basri (in preparation). Both studies contain a considerable number of hot DAs that were detected in the *ROSAT* survey, in addition to a significant overlap with one another. Kidder (1991, hereafter K91) analysed the line profiles of 101 hot DAs using an extension of the grid of models calculated by Wesemael et al. (1980), whereas Finley et al. (hereafter FKB) employ models generated using the code discussed by Koester (1991). Both K91 and FKB use detailed fits to observed Balmer line profiles to determine $T_{\rm eff}$ and log g. Bergeron, Saffer & Liebert (1992) have discussed some systematic effects arising from different theoretical formalisms used to treat Balmer transitions, in particular those of the higher excited levels. While their work promises to lead eventually to a more precise modelling of line profiles, the published results are comparable with those of Koester (1991). Furthermore, only six of the stars in the Bergeron et al. sample were detected by *ROSAT*. Consequently, we have chosen to use both the K91 and FKB results to analyse the *ROSAT* DAs independently, so that any systematic effects present in either data set can be made clear.

Table 1 lists the sample of hot DA white dwarfs selected from the *ROSAT* survey detections that have temperature measurements in either the K91 or FKB (or both) samples. The survey count rates are listed for each star, together with any available pointed-phase data from *ROSAT* or *EXOSAT*. The V magnitudes, optical temperatures and gravities are summarized in Table 2, since these are not yet widely available in the literature. As the WFC survey rates were obtained using an automatic background subtraction and source search process (Pounds et al. 1993), we have repeated the data reduction manually to ensure that there are no hidden errors. The primary effect of the manual reduction is a slight increase in the count-rate uncertainty. The survey analysis uses a fixed radius for extraction of the count rates

and then corrects these for the known point response function (prf) of the instrument. The assumption that the prf is the same for each source only holds if the source exposure is completely uniform across the telescope field of view. In general this is not true, because of periods when the detector may be switched off as a result of high geophysical backgrounds in the auroral horns or South Atlantic Anomaly. Hence there is an additional contribution to the count-rate errors which is not included in the survey catalogue data. In performing a manual count-rate determination, we have determined the extent of the prf from the EUV images of each object and then used an extraction radius that includes more than 99 per cent of the source counts. The statistical count-rate errors are increased, because we are subtracting a greater background component from a larger area on the image, but we avoid any hidden systematic errors arising from the assumed prf.

During the survey, the WFC suffered a small gradual drift in its sensitivity (Willingale et al., in preparation). This has been taken into account in the subsequent analysis, and the *ROSAT* observation date of each object is also noted in Table 1. A few objects (e.g. HZ43 and EG187) were observed during the pre-survey calibration and verification phase of the mission. In these cases, there is no calibration drift to consider and we also have P1 count-rate measurements. Feige 24 was not detected in the S1 filter during the survey, but an S1 calibration measurement was made and this is included in the table. *EXOSAT* AlP count rates are also listed (from Paerels & Heise 1989), where they exist, for those stars that have not yet been observed in the P1 filter.

All of the count-rate uncertainties listed in Table 1 are 1σ statistical values. There are also systematic errors associated with the absolute photometric calibration of the instrument which must be taken into account. The largest factor in these errors is the uncertainty in the reference standards used. For *ROSAT* PSPC, S1 and S2, covering wavelengths shorter than 130 Å, proportional counters, the quantum efficiency of which can be calculated theoretically, are used as standards, giving 1σ calibration errors of 10 per cent. At wavelengths longer than 130 Å (WFC P1 and *EXOSAT* AlP filters), reference photodiodes must be used, yielding typical 1σ errors of 15–20 per cent. We include these systematic errors, in addition to the statistical uncertainties, in our subsequent analyses.

3 ANALYSIS OF THE *ROSAT* OBSERVATIONS WITH H + He MODEL ATMOSPHERES

3.1 Model atmosphere calculations

The model atmospheres used in this work were calculated by two different source programs. Homogeneous H + He models utilized the TLUSTY NLTE code of Hubeny (1988), while stratified models were computed using the code by Koester (1991), which assumes that the LTE approximation holds. In general, for the temperatures and gravities spanned by the hot DA sample, this is reasonable (see e.g. Barstow 1990), although a self-reversed emission core, arising from non-LTE effects, has been reported in the Hα line of G191–B2B (Reid & Wegner 1988). Another important consideration is the degree of line blanketing incorporated into the model calculations. Kidder et al. (1992) have demonstrated that the predicted emergent EUV and soft X-ray fluxes from hot DAs below about 30 000 K are sensitive to this. The Koester models are fully blanketed, whereas the TLUSTY calculations only include blanketing from Ly α and Ly β. To test the potential sensitivity of our results to line blanketing, we have made a direct comparison of a pure H TLUSTY model grid with an equivalent grid from the Koester calculations, where the thickness of the hydrogen layer [denoted by the parameter $\log Pg_0$, where $M_{H(\odot)} \approx 5 \times 10^{-23} Pg_0$] is sufficiently large that the He opacity is negligible ($\log Pg_0 = 10$). In Fig. 2 we show the predicted count rates for a nominal $V = 15.0$ white dwarf with zero H I column in the PSPC, S1 and S2 bands, for the TLUSTY (dashed lines) and Koester (solid curves) models. In the PSPC and S1 filters, the differences are negligible above 30 000 K. In S2, however, the difference is about 30 per cent at 30 000 K and only becomes very small at about 35 000 K. A 30 per cent error in the S2 count rate corresponds to a potential over- or underestimate of about 500–1000 K in a temperature determination. When combined with the other filter measurements, the effect of this error will be reduced substantially. We note that Kidder et al. (1992) found similar differences in their analysis at 25 000 K if unblanketed models were used. From this, we conclude that the unblanketed models are adequate at temperatures above $\approx$ 30 000 K, but we must be aware of the likely systematic errors below this temperature.

Grids of models were calculated to sample fully the parameter space spanned by the DA white dwarfs in the *ROSAT* sample. Table 3 summarizes the values of $T_{\rm eff}$, $\log g$ and He:H or $\log Pg_0$ covered. For the stratified models a fine temperature spacing was used between 20 000 and 30 000 K, since the emergent EUV and X-ray fluxes change most rapidly with increasing temperature in that range. It was not necessary to include this level of sampling in the homogeneous grid because of the limitations in the usefulness of models below 30 000 K discussed above.

3.2 Model fitting

Fits of both homogeneous and stratified models to the observed count rates were made using the package SFIT, which is part of the data analysis package ASTERIX (Saxton 1991), provided for *ROSAT* data reduction in the UK. This program compares predicted count rates, after folding model atmosphere spectra through each instrumental response and interstellar absorption, with observed values in each filter and instrument. A χ^2 statistic is then calculated, which determines the quality of agreement between data and predictions, taking into account the uncertainties in the measured count rates. The program searches through the range of all free parameters to determine the best fit and associated errors. A valid analysis requires that the number of degrees of freedom (ν), that is the number of data points minus the number of free parameters, be greater than or equal to one. There are five variables that determine the predicted EUV and X-ray fluxes for each of our model structures: $T_{\rm eff}$, interstellar H I column ($N_{\rm H}$), $\log g$, helium opacity (He:H or $\log Pg_0$) and a distance/radius-related normalization constant.

Since we only have three (or at most four) independent data points from the EUV/X-ray observations, additional information is required from other sources to specify some

Table 1. Observed *ROSAT* PSPC, WFC and *EXOSAT* CMA count rates (s^{-1}) and associated statistical errors.

WD no.	Obs. date (MJD)	PSPC	PSPC error	S1	S1 error	S2	S2 error	P1/AlP	P1/AlP error
0004+330	49179	2.52	0.12	0.123	0.018	0.0591	0.0077	0.0244 (A)	0.0026
0050−332	48224	3.19	0.19	0.531	0.041	1.702	0.051	1.18 (A)	0.02
0131−164	48179	1.745	0.195	0.230	0.026	0.612	0.065		
0147+674	48111	0.158	0.020	0.0243	0.0082	0.0504	0.0150		
0232+035[1]	48183	0.014	–	0.0049	0.0023	0.704	0.028		
0320−539	PV/Cal	0.230	0.076	0.0641	0.0116	0.187	0.021	0.093 (A)	0.004
0346−011	48109	2.086	0.071	0.228	0.016	0.463	0.028		
0347+171[2]	48113	1.11	0.25	0.340	0.020	1.040	0.029	0.792 (A)	0.013
0457−281	48116	0.106	0.029	0.118	0.015	2.537	0.257		
0501+527[3]	48125	0.040	0.022	0.0650	0.0147	2.718	0.0405	23.1 (A)	0.1
0548+000	48130	0.862	0.061	0.0834	0.0111	0.0865	0.0207	0.014 (A)	0.002
0549+158	48130	2.800	0.113	0.565	0.020	2.119	0.042	1.44 (A)	0.01
0631+107	48141	0.280	0.035	0.0621	0.0110	0.165	0.036		
0642−166	48146	19.730	0.290	2.842	0.036	7.586	0.072		
0651−020	48150	0.682	0.055	0.080	0.012	0.271	0.028		
1031−114	48211	0.242	0.027	0.048	0.012	0.0874	0.0335		
1033+464	48175	0.294	0.026	0.051	0.006	0.199	0.012		
1109+244	48204	0.508	0.042	0.106	0.021	0.098	0.027		
1123+189	48211	0.436	0.033	0.153	0.014	0.753	0.039		
1234+482	48210	1.852	0.061	0.403	0.020	1.580	0.041		
1254+223	PV/Cal	7.64	0.16	1.11	0.05	4.268	0.208	1.5 (P)	0.04
1314+293	PV/Cal	87.17	0.41	14.93	0.10	40.20	0.10	9.21 (P)	0.07
1620−391	48117	0.969	0.0054	0.215	0.021	0.543	0.027	0.095 (A)	0.005
1636+351	48112	0.468	0.029	0.033	0.017	0.0562	0.0266		
1658+440	48115	0.233	0.030	0.061	0.020	0.183	0.022	0.128(A)	0.013
1800+683	48180	0.812	0.237	0.034	0.003	0.009	0.008		
1845+019	48146	1.423	0.075	0.201	0.016	0.686	0.034		
2028+390	48196	0.058	0.016	0.015	0.013	0.057	0.025	0.0081 (A)	0.0017
2111+498	48220	1.282	0.065	0.303	0.013	1.231	0.022	0.65 (A)	0.02
2309+105	48219	6.467	0.114	1.112	0.027	3.95	0.051	1.44 (A)	0.03

Notes: (1) PSPC rate is maximum likelihood 2σ *upper* limit; S1 rate is PV/Cal data; (2) rates are after subtraction of K-star component and removal of eclipses (see Barstow et al. 1992); (3) Al/P count rate has large systematic uncertainties (see Barstow et al. 1993).

of the parameters. It is straightforward to normalize the spectra using the V magnitudes of the stars. Typical published errors of ≈ 0.01–0.03 on the V-magnitude determinations have only a 1–3 per cent effect on the predicted fluxes, very much smaller than the other uncertainties in the analysis. Gravity determinations exist for all of the stars in our sample. Since predicted fluxes are insensitive to the choice of log g within the normal range found for hot DA white dwarfs, we have fixed log g at the optically determined value in our analysis. For example, in a given model calculation, a change in the value of log g from 7.5 to 8.0 results in a maximum change of only ≈ 7.5 per cent in the predicted EUV and X-ray count rates within the DA temperature range. Experimental errors in the determination of log g are usually ± 0.1 or less.

Even with V-magnitude and surface gravity information incorporated into the analysis, there are still three remaining variables, $T_{\rm eff}$, $N_{\rm H}$ and He fraction or H-layer mass. Where only three photometric fluxes are available, the spectral fitting is first carried out with the value of $T_{\rm eff}$ fixed successively at the nominal value and then at the bounds as determined from the optical work. If a good fit is achieved then the ranges of $N_{\rm H}$ and He opacity allowed by the optical temperatures can be determined. Secondly, either $N_{\rm H}$ or the He opacity is fixed and a series of fits performed, gradually increasing that parameter, to explore the full range of values allowed by the EUV/X-ray data alone. This is a particularly important exercise if the fits at the optically determined temperature are poor, as good agreement between data and model predictions may be found in a different temperature range. In principle, when four or more data points are available, all three variables can be allowed to remain as free parameters in the spectral fitting so that their values and allowed ranges can be determined. However, the χ^2 minimum is often ill-defined and it is still necessary to follow the approach outlined above.

We have carried out detailed comparisons between the observed count rates and the model atmosphere predictions for each star in our sample. It is necessary to define in this analysis what is a good fit to the data and what is not. To do this in an objective way, we consider the probability that a particular value of the reduced χ^2 ($\chi^2_{\rm r} = \chi^2/\nu$) can occur by

Table 2. Optically determined temperatures, gravities and V magnitudes for the sample.

WD no.	Alt. Name		FKB Data		K91 data	
		m_V [1]	T_{eff} ($\pm1\sigma$)	log g ($\pm1\sigma$)	T_{eff} ($\pm1\sigma$)	log g ($\pm1\sigma$)
0004+330	GD2	13.85	47,297 (692)	7.650 (0.090)	48,100 (1,800)	7.80 (0.16)
0050−332	GD659	13.37	34,551 (252)	7.763 (0.069)	36,000 (700)	7.95 (0.27)
0131−164	GD984	13.96			45,800 (3,700)	7.90 (0.43)
0147+674	GD421	14.41	29,631 (189)	7.573 (0.067)	31,000 (200)	7.75 (0.05)
0232+035	Feige 24	12.56			59,800 (3,400)	7.45 (0.51)
0320−539	LB1663	14.5			30,400 (3,300)	7.40 (0.67)
0346−011	GD50	14.04	38,088 (91)	8.868 (0.042)	43,400 (1,700)	> 9
0347+171	V471 Tau	13.65			34,200 (600)	8.80 (0.28)
0457−281[2]	RE	13.99			60,700 (1,450)	7.78 (0.090)
0501+527	G191-B2B	11.73	57,314 (750)	7.497 (0.065)	58,100 (1,300)	7.45 (0.015)
0548+000	GD257	14.79	45,561 (1,147)	7.669 (0.162)	46,200 (3,000)	7.85 (0.24)
0549+158	GD71	13.03	32,045 (148)	7.721 (0.052)	33,000 (700)	7.80 (0.27)
0631+107	KUV	13.82			27,200 (400)	8.00 (0.13)
0642−166	Sirius B	7.8			24,700 (1,000)	8.65 (0.3)
0651−020	GD80	14.8	32,779 (195)	8.003 (0.060)	33,800 (1,000)	8.00 (0.21)
1031−114	EG70	13.01			25,400 (200)	7.95 (0.23)
1033+464	GD123	14.34	28,922 (166)	7.835 (0.059)	30,200 (300)	7.95 (0.06)
1109+244	PG	15.98	41,232 (546)	7.424 (0.085)		
1123+189	PG	14.06	51,396 (913)	7.700 (0.097)		
1234+482	PG/HS	14.5			56,200 (1,500)	7.65 (0.15)
1254+223	GD153	13.38	37,886 (292)	7.722 (0.060)	39,400 (1,400)	7.75 (0.29)
1314+293	HZ43	12.99	49,941 (824)	8.136 (0.091)	54,000 (4,400)	7.6 (0.38)
1620−392	CoD -38° 10980	11.00	24,128 (186)	8.111 (0.035)	24,800 (1,700)	7.45 (0.27)
1636+351	KUV	14.91	35,938 (394)	7.802 (0.083)	37,200 (1,200)	7.95 (0.17)
1658+440	PG	15.02				
1800+686	KUV	14.74			46,200 (1,700)	7.80 (0.26)
1845+019	BPM93487	12.95	28,206 (185)	7.724 (0.052)	30,000 (400)	7.90 (0.18)
2028+390	GD391	13.38			24,800 (400)	7.95 (0.22)
2111+498	GD394	13.08	37,378 (268)	7.829 (0.056)	39,800 (1,100)	8.05 (0.31)
2309+105	GD246	13.09	54,987 (931)	7.708 (0.085)	56,200 (1,700)	7.8 (0.32)

Notes: (1) All V magnitudes from Kidder (1991), except KUV objects which are from Wegner et al. (1990); (2) not from Kidder (1991); see Barstow et al. (1993b) – same models used for analysis.

chance. We consider a good fit to correspond to a probability of 0.1 or greater (i.e. 90 per cent confidence) and a bad fit a probability of 0.01 or less (99 per cent confidence). In between, the fits are not necessarily good, but we cannot exclude the models with high confidence. Table 4 lists the value of χ^2_r corresponding to probabilities of 0.32, 0.1, 0.01 and 0.001 (confidence levels of 68 per cent = 1σ, 90, 99 and 99.9 per cent $\approx 3\sigma$) for several values of ν. Taking as an example a spectral analysis with $\nu = 1$, a 'good' fit requires χ^2_r to be less than 2.71, but the value would need to exceed 6.63 before we could exclude any model with certainty. Assignment of parameter ranges, when an acceptable fit is achieved, follows a similar argument. All of the bounds quoted here correspond to a 1σ confidence level. The results of the spectral fitting exercise are summarized separately in Tables 5 and 6 for the homogeneous and stratified models respectively. Tables 5(a) and 6(a) show the results for fits to the EUV and X-ray data alone, whereas Tables 5(b) and 6(b) show the fits for the optical temperature limits and the corresponding N_H and He abundance or H-layer mass values.

3.3 Results for homogeneous models

We consider here the results of the spectral fitting under the assumption that the white dwarf atmospheres are homogeneous mixtures of H and He. It is possible to divide the white dwarf sample into three groups according to how well the model predictions agree with the observations. The main group comprises those stars for which good fits are obtained within the allowed optical temperature ranges. In each case the He abundance usually lies within the range $\approx 0\text{–}4 \times 10^{-5}$ (number fraction), although three stars (GD2, GD50 and GD257) have abundances a factor of 10 higher (see Fig. 3). Formally, we can only place an upper limit of $\approx 4 \times 10^{-5}$ on He/H for those stars with the lowest abundances, given the experimental errors, but we note that a pure H model is perfectly acceptable for these objects. In a second group, comprising GD984, GD246 and PG1234, it is only possible to achieve a good fit at temperatures considerably lower than the optical values. For the remaining objects with $T_{eff} > 30\,000$ K (G191–B2B, Feige 24, WD 1123+189, WD 1109+244, GD153, V471 Tau and GD394), there are no acceptable spectral fits for any combination of T_{eff}, N_H or

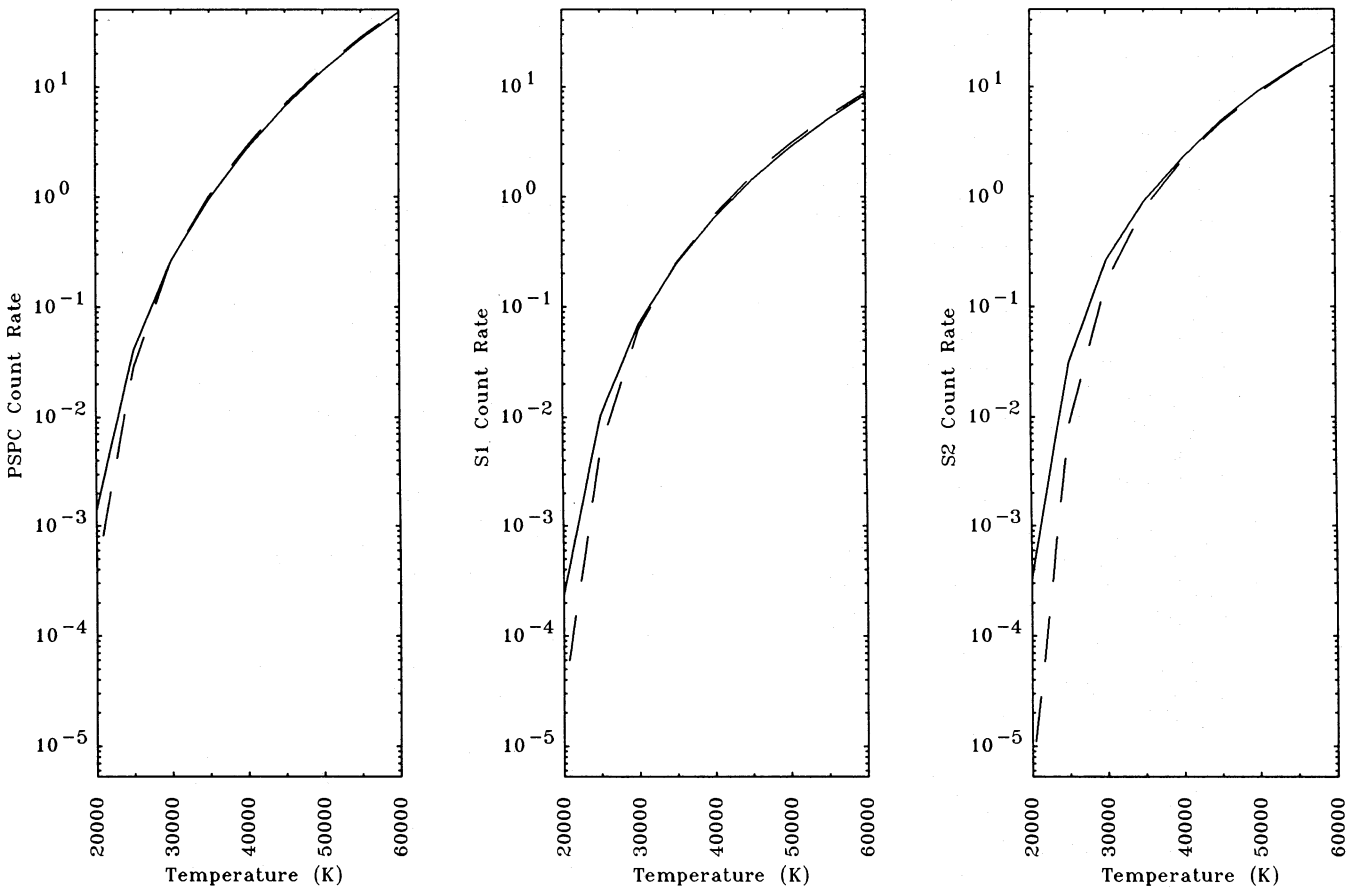

Figure 2. Predicted count rates in the *ROSAT* survey bands for a 15th-magnitude pure H white dwarf. The solid curves represent the blanketed LTE models of Koester (1991) and the dashed curves the partially blanketed NLTE models computed using the code of Hubeny (1988).

Table 3. Model atmosphere grid parameters.

Model type	Temperature grid	log g	Helium abundance or log Pg_0
Homogeneous	20,000–80,000K	7.0–9.0	$0 - 10^{-3}$
Stratified	20,000–60,000K	7.5–8.5	6.5 – 10.0

Table 4. Probability of χ^2_ν exceeding the tabulated values.

	Probability (confidence level)			
ν	0.32 (68% =1σ)	0.1 (90%)	0.01 (99%)	0.001 (99.9% $\approx 3\sigma$)
1	1.00	2.71	6.63	10.83
2	1.15	2.3	4.6	6.91
3	1.17	2.1	3.8	5.4
4	1.18	1.95	3.33	4.6

He/H ratio. Most of the DAs with $T_{\rm eff}$ below 30 000 K (Sirius B, CoD − 39° 10980, GD391 and EG70) do not give good fits either, but this almost certainly arises from the absence of line blanketing in the models, except for EG70, where the discrepancies are too large to be explained in this way. This overall result is illustrated graphically in Fig. 4, where the complete temperature range allowed by the EUV/X-ray data (irrespective of any optical contraints) is plotted against the optically determined values for each star, treating FKB (Fig. 4a) and K91 (Fig. 4b) data separately. Those stars that lie on the equal-temperature line can be adequately interpreted by homogeneous H + He models. In contrast, those objects that lie below, i.e. where the EUV/X-ray temperature is less than the optical value, must have an additional source of opacity in their photospheres that is not accounted for in these models. The stars that do not fit at all appear to be extreme examples of the effect we observe. We note that no objects have EUV/X-ray temperatures that exceed the optical

values. A striking feature of Fig. 4 is that those stars with additional photospheric opacity are mostly hotter than about 40 000 K, whereas those that are in good agreement with nearly pure H models are, in the main, cooler than this.

Comparing the FKB and K91 data on an object-to-object basis, it can be seen that there are systematic differences between the optical temperatures. Those of K91 are typically about 1000 K hotter than the equivalent FKB values. We do not propose to discuss the detailed reasons for this here, but we note that this almost certainly arises from the different codes used to generate the synthetic line profiles, and that the Koester models represent a more complete physical treatment. Clearly, the general picture is unaffected by the choice of optical data set. However, the K91 data imply a need for more photospheric opacity in all stars than is required by the FKB temperatures.

3.4 Results for stratified models

A broadly similar picture is obtained when we use the stratified models instead of the homogeneous grid, and it is possible to divide the white dwarf sample into the same three

Table 5. (a) Spectral fitting with homogeneous models, X-ray + EUV data only.

WD number	Alt. name	χ^2_r	Temperature (K)	He/H	N_H (cm^{-2})
				1σ bounds	
0004+330	GD2	0.9	46,989	2.9×10^{-4}	4.1×10^{19}
			45,640–48,954	$(0.7 - 4.4) \times 10^{-4}$	$(2.8 - 7.3) \times 10^{19}$
0050−332	GD659	0.02	34,227	3.5×10^{-6}	3.4×10^{18}
			32,650–35,900	$0.0 - 2.6 \times 10^{-5}$	$(1.9 - 4.9) \times 10^{18}$
0131−164	GD984	1.6	36,000	3.7×10^{-5}	0.0
			34,900-36,800	$0.0 - 7.4 \times 10^{-5}$	$0.0 - 5.0 \times 10^{18}$
0147+674	GD421	0.0011	30,403	6.3×10^{-5}	0.0
			25,890–37,572	$0.0 - 2.9 \times 10^{-4}$	$0.0 - 4.3 \times 10^{19}$
0232+035	Feige 24	no fit acceptable			
0320−539	LB1663	0.11	29,245	1.1×10^{-6}	0.0
			26,940–30681	$(1.1 - 2.50) \times 10^{-6}$	$0 - 5.1 \times 10^{18}$
0346−011	GD50	0.1	37,375	2.4×10^{-4}	0.0
			34,100–39,600	$(1.3 - 2.9) \times 10^{-4}$	$0.0 - 2.6 \times 10^{19}$
0347+171	V471 Tau	no fit acceptable			
0457−281	RE	no fit acceptable			
0501+527	G191-B2B	no fit acceptable			
0548+000	GD257	1.9×10^{-5}	40,853	6.4×10^{-5}	3.5×10^{19}
			37,320–45,260	$0 - 2.6 \times 10^{-4}$	$(1.8 - 6.05) \times 10^{19}$
0549+158	GD71	1.4	31,498	0.0	1.2×10^{18}
			31,003–32,901	$0.0 - 1.4 \times 10^{-5}$	$0.0 - 2.4 \times 10^{18}$
0631+107	KUV				
0642−166	Sirius B	no fit acceptable			
0651−020	GD80	2.3	35,171	6.2×10^{-5}	0.0
			30,825–36,503	$0.0 - 9.5 \times 10^{-5}$	$0.0 - 1.9 \times 10^{19}$
1031−114	EG70	no fit acceptable			
1033+464	GD123	2.6	27,810	0.0	0.0
			27,282–29,710	$0.0 - 1.2 \times 10^{-5}$	$0.0 - 4.7 \times 10^{18}$
1109+244		no fit acceptable			
1123+189		no fit acceptable			
1234+482	PG, HS	1.9	36,124	0.0	0.0
			35,700–37,030	$0.0 - 9.9 \times 10^{-6}$	$0.0 - 2.7 \times 10^{18}$
1254+223	GD153	no fit acceptable			
1314+293	HZ43	0.7	50,918	0.0	4.9×10^{18}
			50,138–52,375	$0 - 6.1 \times 10^{-5}$	$(2.2 - 27) \times 10^{18}$
1620−392	CoD -38 10980	no fit acceptable			
1636+351		4×10^{-8}	41,207	3.0×10^{-4}	4.9×10^{17}
			35,032–50,038	$0.0 - 1 \times 10^{-3}$	$0.0 - 9.5 \times 10^{19}$
1658+440	PG	0.91	30,324	0.0	0.0
			28,187–31,376	$0.0 - 1.7 \times 10^{-5}$	$0.0 - 3.1 \times 10^{19}$
1800+686	KUV	3.3	50,329	0.0	1.3×10^{20}
			46,620–55,380	$0.0 - 1 \times 10^{-3}$	$(0.3 - 1.5) \times 10^{20}$
1845+019	BPM93487	2.9	30,386	1.9×10^{-5}	0.0
			27,963–32,060	$0.0 - 6.1 \times 10^{-5}$	$0.0 - 1.1 \times 10^{19}$
2028+390	GD391	no fit acceptable			
2111+498	GD394	no fit acceptable			
2309+105	GD246	5.4	37,083	0.0	8.6×10^{18}
			36,230–37,860	$0.0 - 1.1 \times 10^{-5}$	$(6.5 - 9.6) \times 10^{18}$

Table 5. (b) Spectral fitting with homogeneous models; temperature fixed within optically determined boundaries.

WD number	Alt. name	χ^2_r	Temperature (K)	He/H	N_H (cm^{-2})
0004+330	GD2	0.5	46,605	2.1×10^{-4}	5.9×10^{19}
		0.5	47,989	5.1×10^{-4}	3.7×10^{19}
0050−332	GD659	0.01	34,298	3.9×10^{-6}	3.3×10^{18}
		0.05	34,804	6.7×10^{-6}	3.2×10^{18}
0131−164	GD984	no fit within optical range			
0147+674	GD421	0.03	29,442	3.1×10^{-5}	0.0
		0.02	29,820	3.5×10^{-5}	0.0
0232+035	Feige 24	no fit acceptable			
0320−539	LB1663	3.5	27,100	1.1×10^{-6}	0.0
		15.0*	33,700	6.2×10^{-5}	8.0×10^{17}
0346−011	GD50	0.25	37,997	2.6×10^{-4}	0.0
		0.35	38,179	2.6×10^{-4}	0.0
0347+171	V471 Tau	no fit acceptable			
0457−281	RE	no fit acceptable			
0501+527	G191-B2B	no fit acceptable			
0548+000	GD257	1.0	44,414	2.3×10^{-4}	2.6×10^{19}
		4.3	46,708	5.0×10^{-4}	2.3×10^{19}
0549+158	GD71	1.1	31,897	1.7×10^{-6}	1.6×10^{18}
		1.4	32,193	5.3×10^{-6}	1.4×10^{18}
0631+107	KUV				
0642−166	Sirius B	no fit acceptable			
0651−020	GD80	4.0	32,584	3.0×10^{-5}	0.0
		2.7	32,974	3.0×10^{-5}	0.0
1031−114	EG70	no fit acceptable			
1033+464	GD123	4.4	28,856	6.4×10^{-6}	0.0
		4.9	29,088	7.6×10^{-6}	0.0
1109+244	PG	no fit acceptable			
1123+189	PG	no fit acceptable			
1234+482	PG/HS	no fit within optical range			
1254+223	GD153	no fit acceptable			
1314+293	HZ43	4.3	49,100	1.2×10^{-5}	3.3×10^{18}
		0.51	50,760	2.9×10^{-5}	4.7×10^{18}
1620−392	CoD -38° 10980	no fit acceptable			
1636+351	KUV	1.9	35,544	0.0	3.7×10^{18}
		0.9	36,332	2.6×10^{-7}	4.4×10^{18}
1658+440	PG	no optical temperature determination			
1800+686	KUV	6.8*	46,620	0.0	2.9×10^{19}
		4.7	47,900	0.0	1.3×10^{20}
1845+019	BPM93487				
2028+390	GD391	no fit acceptable			
2111+498	GD394	no fit acceptable			
2309+105	GD246	no fit within optical range			

*Optical temperature limit outside the range of acceptable fits.

categories, although not necessarily containing the same members (see Tables 6a and b). The main groups (which were consistent with near pure H models above) give good fits for stratified models with relatively thick H-layer masses (Fig. 5). It is not possible to distinguish between the two alternative structures, but it is clear that the role of He as an opacity source is minimal. It is possible, however, to establish a lower limit of $\approx 1 \times 10^{-13} M_\odot$ to the allowed H-layer mass. This result is telling us that the layer mass is sufficiently thick that even the EUV and X-ray fluxes, emerging from the deeper layers, are originating from almost pure H material. There is a substantial gap between the observed layer masses and the lower detection limit (dashed line), which demonstrates that the observed values are not an observational selection effect. If they exist, stars with lower H-layer masses should have been detected. We note that Sirius B falls below the detection limit marked (for $\log g = 7.5$) because of its unusually high gravity ($\log g = 8.5$) when compared with the rest of the sample.

The other two groups analogous to those arising from the homogeneous analysis are more difficult to interpret. When only the survey data are available for these stars it is possible

to achieve a good fit, with suitable choices of N_H and M_H at temperatures within the allowed optical range (e.g. PG1123 and PG1234). Relatively high values of both parameters are always required, with N_H generally exceeding 1×10^{19} cm^{-2}. However, when supplementary data are available in the form of a P1 or AlP count rate or as an independent determination of N_H, good fits are no longer possible within the optical temperature range, and in some cases are impossible for any temperature. Furthermore, it is notable that the majority of white dwarfs that yield good fits

Table 6. (a) Spectral fitting with stratified models, X-ray + EUV data only.

WD number	Alt. name	χ^2_r	Temperature (K)	M_H ($\times 10^{-13} M_\odot$) 1σ bounds	N_H (cm^{-2})
0004+330	GD2	no fit acceptable			
0050−332	GD659	0.6	32,507	13	4.5×10^{18}
			31,693−35,270	2.8−>20	$(3.3 - 7.0) \times 10^{18}$
0131−164	GD984	no fit acceptable			
0147+674	GD421	0.3	28,443	22	2.1×10^{19}
			25,995−>60,000	0.25−>22	$0.0 - 8.5 \times 10^{19}$
0232+035	Feige 24	no fit acceptable			
0320−539	LB1663	0.1	29,188	6.5	4.8×10^{18}
			27,841−29,944	6.5->24	$0 - 1.6 \times 10^{19}$
0346−011	GD50	no fit acceptable			
0347+171	V471 Tau	0.4	30,906	0.33	3.1×10^{18}
			29,577−32,799	0.15−0.67	$0.0 - 2.7 \times 10^{19}$
0457−281	RE	no fit acceptable			
0501+527	G191-B2B	no fit acceptable			
0548+000	GD257	0.7	53,558	0.86	6.7×10^{19}
			37,230−>60,000	0.52−>23	$(4.2 - 8.8) \times 10^{19}$
0549+158	GD71	2.2	31,691	3.8	3.8×10^{18}
			30,499−34,370	0.85−>20	$(1.4 - 6.5) \times 10^{18}$
0631+107	KUV	0.01	27,308	1.9	4.9×10^{18}
			26,060−>60,000	0.052−>5.6	$0.0 - 4.9 \times 10^{19}$
0642−166	Sirius B	2.4	23,205	1	3.5×10^{18}
			22,290−24,271	0.42−>1	$0.0 - 9.3 \times 10^{18}$
0651−020	GD80	no fit acceptable			
1031−114	EG70	no fit acceptable			
1033+464	GD123	1.9	27,856	7.9	0.0
			27,458− >60,000	0.14−>13	$0.0 - 2.7 \times 10^{19}$
1109+244	PG	1.9	43,358	2.8	3.5×10^{19}
			25,000−>60,000K	0.66−>38	$(2.1 - 4.7) \times 10^{19}$
1123+189	PG	0.5	43,500	0.6	1.5×10^{19}
			31,000−>60,000	0.19−1.8	$0 - 2 \times 10^{19}$
1234+482	PG/HS	0.1	35,852	3.3	0.0
			35,015−>60,000	0.28−>27	$0.0 - 2.5 \times 10^{19}$
1254+223	GD153	no fit acceptable			
1314+293	HZ43	2.9	52,238	0.98	6.0×10^{18}
			49,124−54,580	0.61−10	$(3.8 - 8.3) \times 10^{18}$
1620−392	CoD -38° 10980	0.2	27,097	0.74	1.9×10^{19}
			24,600−>60,000	0.043−1.8	$(0.8 - 4.3) \times 10^{19}$
1636+351	KUV	1.5	37,660	24	6.0×10^{19}
			33,850−46,800	0.27−>24	$(0.3 - 1.5) \times 10^{20}$
1658+440	PG	0.007	30,112	5.6	2.5×10^{18}
			28,187−31,376	1.6−15	$0.0 - 3.2 \times 10^{19}$
1800+686	KUV	0.6	49,978	33	1.4×10^{20}
			46,390−>60,000	1.6−>33	$(1.3 - 1.6) \times 10^{20}$
1845+019	BPM93487	no fit acceptable			
2028+390	GD391	0.1	27,989	0.43	2.3×10^{19}
			21,520−>60,000	0.023−>3.7	$0 - 5.2 \times 10^{19}$
2111+498	GD394	0.23	31,949	1.4	7.4×10^{18}
			29,934−33,969	1.2−2.4	$(3.2 - 30) \times 10^{18}$
2309+105	GD246	1.3	46,518	0.86	16×10^{18}
			34,432−50637	0.6−4.6	$(8.2 - 21) \times 10^{18}$

Table 6. (b) Spectral fitting with stratified models; temperature fixed within optically determined boundaries.

WD number	Alt. name	χ^2_r	Temperature (K)	M_H ($\times 10^{-13} M_\odot$)	N_H (cm^{-2})
0004+330	GD2	no fit acceptable			
0050−332	GD659	1.1	34,298	3.0	6.0×10^{18}
		1.4	34,804	3.0	6.4×10^{18}
0131-164	GD984	no fit acceptable			
0147+674	GD421	0.3	29,442	5.4	2.6×10^{19}
		0.3	29,820	5.4	2.8×10^{19}
0232+035	Feige 24	no fit acceptable			
0320−539	LB1663	no fit within optical range			
0346−011	GD50	no fit acceptable			
0347+171	V471 Tau	no fit within optical range			
0457−281	RE	no fit acceptable			
0501+527	G191-B2B	no fit acceptable			
0548+000	GD257	0.9	44,414	2.6	6.3×10^{19}
		0.7	46,708	1.6	6.2×10^{19}
0549+158	GD71	1.1	31,897	3.8	4.1×10^{18}
		1.1	32,193	3.2	4.5×10^{18}
0631+107	KUV	0.02	26,800	2.6	1.5×10^{18}
		0.01	27,600	1.5	6.3×10^{18}
0642−166	Sirius B	3.0	23,700	0.6	5.4×10^{18}
		7.1*	25,700	0.32	2.1×10^{19}
0651−020	GD80	no fit acceptable			
1031−114	EG70	no fit acceptable			
1033+464	GD123	2.6	28,856	2.9	4.1×10^{18}
		2.7	29,088	2.9	5.0×10^{18}
1109+244	PG	2.1	40,686	8.3	3.2×10^{19}
		2.1	41,778	5.0	3.3×10^{19}
1123+189	PG	0.5	50,400	0.36	1.0×10^{19}
		0.5	52,309	0.36	1.0×10^{19}
1234+482	PG/HS	0.5	54,700	0.49	1.8×10^{19}
		0.15	57,700	0.4	1.7×10^{19}
1254+223	GD153	no fit acceptable			
1314+293	HZ43	2.4	49,100	1.3	4.2×10^{18}
		2.1	50,760	1.1	5.2×10^{18}
1620−392	CoD -38° 10980	4.0	23,942	3.9	3.8×10^{18}
		2.8	24,314	2.0	6.5×10^{18}
1636+351	KUV	2.6	35,544	13.0	4.3×10^{18}
		1.8	36,332	11.0	5.1×10^{18}
1658+440	PG	no optical temperature determination			
1800+686	KUV	4.1*	46,390	0.83	1.3×10^{20}
		1.7	47,900	32.0	1.4×10^{20}
1845+019	BPM93487	no fit acceptable			
2028+390	GD391	0.5	24,400	2.7	7.7×10^{18}
		0.2	25,200	2.5	1.2×10^{19}
2111+498	GD394	no fit within optical range			
2309+105	GD246	no fit within optical range			

*Optical temperature limit outside the range of acceptable fits.

with high H-layer masses also have low H I columns with N_H less than about 3×10^{18} cm^{-2}. It seems unlikely that the other DAs have high columns, but it cannot be ruled out.

From the evidence outlined above, we arrive at the same general picture for the composition of DA white dwarf atmospheres, irrespective of the choice of model structure. The majority of white dwarfs in the sample, which are mainly cooler than about 40 000 K, appear to have nearly pure H atmospheres. Whether we choose to describe this as homogeneous H + trace He or stratified with a relatively thick H layer is immaterial. Only the star HZ43 in the group of stars hotter than 50 000 K has a nearly pure H envelope, the rest requiring additional material in their atmospheres to explain the observed EUV and X-ray count rates. Since we have demonstrated that in general neither homogeneous nor stratified H + He models are able to provide the required opacity, we can only conclude that traces of elements heavier than H and He must be present in most of these stars.

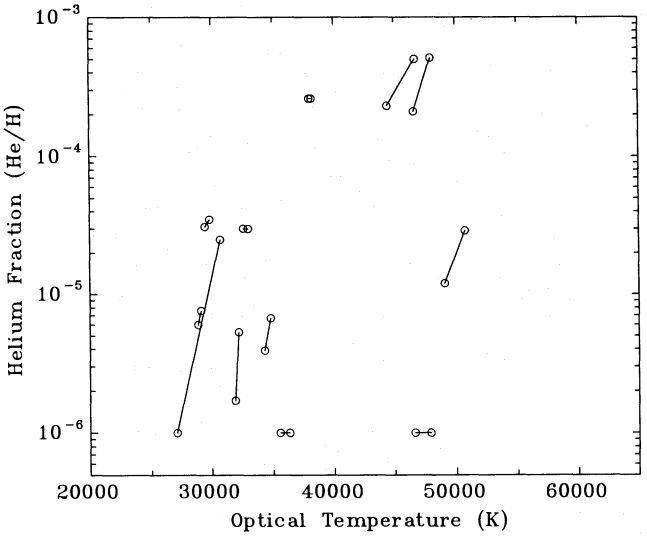

Figure 3. The range of He abundances allowed by the X-ray and EUV data for those white dwarfs for which good fits to homogeneous H + He models are obtained within the optically determined temperature bounds. Each pair of open circles, joined by a bar, marks the values of the He/H fraction at the $\pm 1\sigma$ limits on the optically determined temperature.

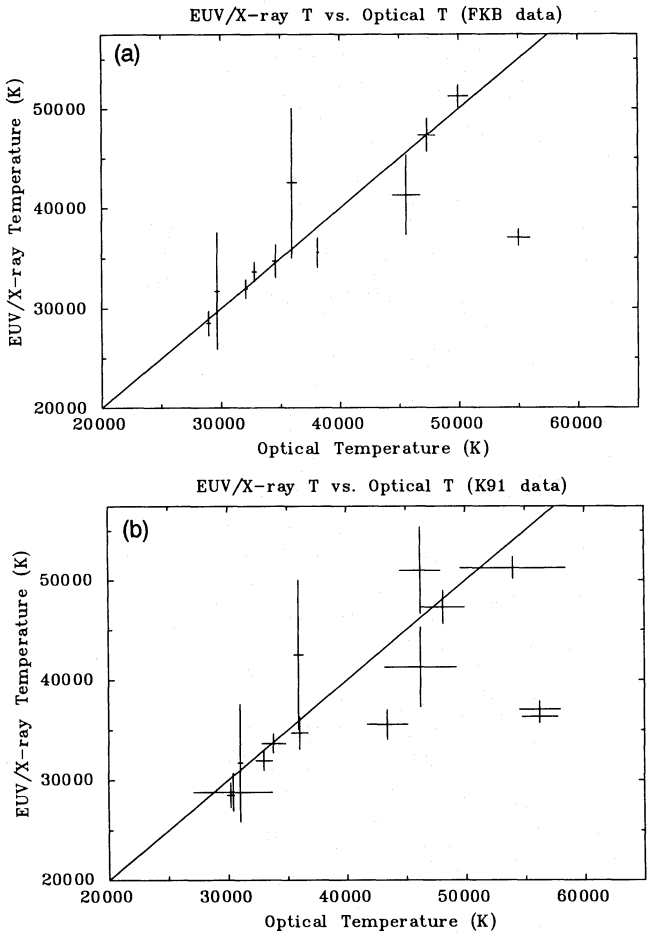

Figure 4. The temperature range allowed by the X-ray and EUV data for those white dwarfs for which good fits to homogeneous H + He models are obtained within the parameter space covered by the model grid, compared to the optically determined temperatures of Finley et al. (in preparation, FKB, panel a) and Kidder (1991, K91, panel b).

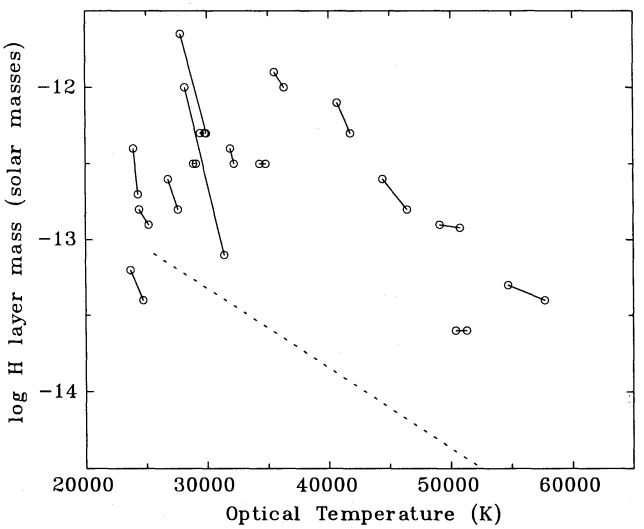

Figure 5. The range of H-layer masses allowed by the X-ray and EUV data for those white dwarfs for which good fits to stratified H + He models are obtained within the optically determined temperature bounds. Each pair of open circles, joined by a bar, marks the values of the layer mass at the $\pm 1\sigma$ limits on the optically determined temperature. The dashed line indicates the layer mass (calculated for a typical white dwarf of log $g = 7.5$) below which white dwarfs cannot be detected by *ROSAT*.

3.5 Non-detections of hot DA stars

It is not our purpose here, nor is it appropriate in this paper, to carry out a systematic statistical survey of the detections and non-detections of DA white dwarfs in the *ROSAT* survey. Nevertheless, there is a striking result that deserves some discussion here. In studying the data of FKB and K91, we find that no DA in their lists with $T_{\rm eff}$ above 60 000 K was detected in the survey, and that many of those in the 50 000–60 000 K range are also not seen. The total number of these non-detections (9, see Table 7) is larger than the number actually detected in the survey between 50 000 and 60 000 K. In the absence of any source(s) of opacity, interstellar or photospheric, these objects should all be luminous EUV/X-ray sources, but they are not. It may be that they all lie along lines of sight where the interstellar absorption is high enough to prevent their detection. In the light of the above discussion (in Sections 3.3 and 3.4), however, an alternative explanation may be that radiative levitation of heavy elements has increased the photospheric opacity to the level at which the EUV/X-ray flux is completely blocked.

A good example for which the latter explanation appears to be true is the star WD 0343 − 007 (61 700 K, $V = 14.91$), which lies ≈ 40 arcmin away from the cooler object GD50 (38 000 K, $V = 14.04$) which was detected. Fig. 6 shows the $2° \times 2°$ WFC image containing both stars. The position of WD 0343 − 007 is shown by the circle. The information on the column density derived from the analysis of the GD50 data can be used to constrain that in the direction of WD 0343 − 007. From the effective temperatures of the stars, we have estimated their luminosities and distances (using the bolometric corrections for a pure H atmosphere given by Wesemael et al. 1980). GD50 lies at a distance of ≈ 75 pc and WD 0343 − 007 lies at ≈ 164 pc. Hence the maximum H I column of $\approx 2.6 \times 10^{19}$ cm^{-2} obtained for GD50 suggests that the line-of-sight column to

Table 7. White dwarfs hotter than 50 000 K not detected in the survey.

WD no.	m_V	FKB Data T_{eff} ($\pm 1\sigma$)	K91 data T_{eff} ($\pm 1\sigma$)
0343−007	14.91	61,696 (1,260)	
0836+237	16.7	51,856 (1,290)	54,200 (4,800)
0939+262	14.6	64,547 (1,533)	
1210+533	14.12		52,400 (3,400)
1532+033	15.9	58,005 (1,993)	
1548+405	15.9	53,423 (1,015)	
2046+396	14.43	57,387 (1,676)	
2244+031	16.36	54,987 (931)	
2353+026	15.8	60,966 (1,226)	

WD 0343 − 007 should be about 5.7×10^{19} cm^{-2}, a value consistent with the maps of Frisch & York (1983).

From the survey data, we have derived 3σ upper limits (using Bayesian statistics) to the count rates from WD 0343 − 007 of 0.01 and 0.016 count s^{-1} in S1 and S2 bands respectively. To explain the absence of a detection of this star, the H I column would have to be greater than 1.5×10^{20} cm^{-2}, even with a relatively high He/H ratio (assuming a homogeneous atmosphere) of 1×10^{-3}. Given the proximity of the star to GD50, it is unlikely that the column density is so high. Furthermore, at this level He would begin to be detectable in the optical spectrum of the star, but is not seen in this example (e.g. Holberg et al. 1989). Consequently, it appears that WD 0343 − 007 is not detected as a result of photospheric rather than interstellar opacity. We cannot yet rule out the possibility that He makes a significant contribution to the photospheric opacity, but, if the star is similar to the other hot DAs that we have studied, the opacity is most likely to come from heavier elements.

4 A COMPARISON OF ABSOLUTE EUV/X-RAY FLUXES FROM THE SAMPLE

We have demonstrated that, for most DAs hotter than about 40 000 K, some opacity source, in addition to He, is required to explain the observed *ROSAT* count rates. Further interpretation of the data is restricted by the absence of suitable models containing trace metals. We are working to develop these models, although we recognize that photometric data of the kind provided by *ROSAT* will never be able to determine unambiguously the precise nature and abundance of the opacity sources. These can only be found by spectroscopic observations. Nevertheless, we can study the emergent EUV/X-ray fluxes for our sample of white dwarfs and, by comparing data for stars of similar temperature, gain information about whether the opacities are a monotonic function of temperature or show a range of values.

In order to make such comparisons, it is necessary to estimate the absolute fluxes from the observed count rates in each band. As discussed in the context of spectral fitting, the V magnitude is a useful normalization point, as it is accurately known. Important information may also be present in the downward slope of the EUV fluxes towards higher photon energies. However, this is obscured in the disparate effective areas of each instrument and filter combination (see Fig. 1). An estimate of the EUV/X-ray flux in each band can be made by dividing the observed count rate by some nominal average effective area ($A_{\rm eff}$) at the mean energy (E) of the instrumental bandpass. Since white dwarf spectra decrease steeply throughout the energy range of each filter, the values of $A_{\rm eff}$ and E must be dependent on the actual spectral shape, to some extent. This approach does, however, provide a good first-order estimate of the incident flux. The values of $A_{\rm eff}$ (cm^2) and E (keV) used are, respectively, 7 and 0.085 (S2), 8 and 0.14 (S1), and 190 and 0.2 (PSPC). Use of the V-magnitude normalization then gives estimates of the relative emergent EUV/X-ray flux from each star as a function of energy.

As we are only concerned with the relative fluxes from star to star, for ease of handling we choose a value of the normalization constant that produces a V-magnitude correction factor of 1 for $V = 11.0$. Hence we can define the relative emergent flux as

$$C_E = 4 \times 10^{-5} C_{\rm obs} / (E A_{\rm eff} \times 10^{-0.4 m_V}).$$

In Fig. 7 we display the relative fluxes for the survey bands (S2, S1 and PSPC) as a function of temperature for each star. Also shown are the values predicted for a DA white dwarf with a canonical pure H composition and an H I column of 2.5×10^{18} cm^{-2}, a value typical of the DAs in the sample. It is instructive to look first at the group of white dwarfs with temperatures less than 40 000 K. Clearly, a majority of stars have fluxes that are very close to those predicted for a pure H atmosphere with relatively low column. In most cases, as can be seen by comparison with Tables 5 and 6, the modest differences arise from higher or lower column densities. Where we see larger differences, notably for GD394, EG70 and KUV1636, there is clearly substantial additional opacity of some kind. If interstellar, then any extra absorption will have a greater effect on the fluxes at the longest wavelengths. KUV1636 is a good example, where the observed fluxes show decreasing departures from the pure H model with increasing band energy. In contrast to this, GD394 shows a flux decrement that has a roughly constant factor in each band. As we have demonstrated in the detailed spectral fitting analysis, this is a result of photospheric opacity. It becomes more difficult to detect any photospheric effects when the interstellar opacity is large, for example as in KUV18004.

Further information can be gained from the spectral slopes, determined by taking the ratios of S2:PSPC and S1:PSPC fluxes (Fig. 8). In Fig. 8 the dashed lines again

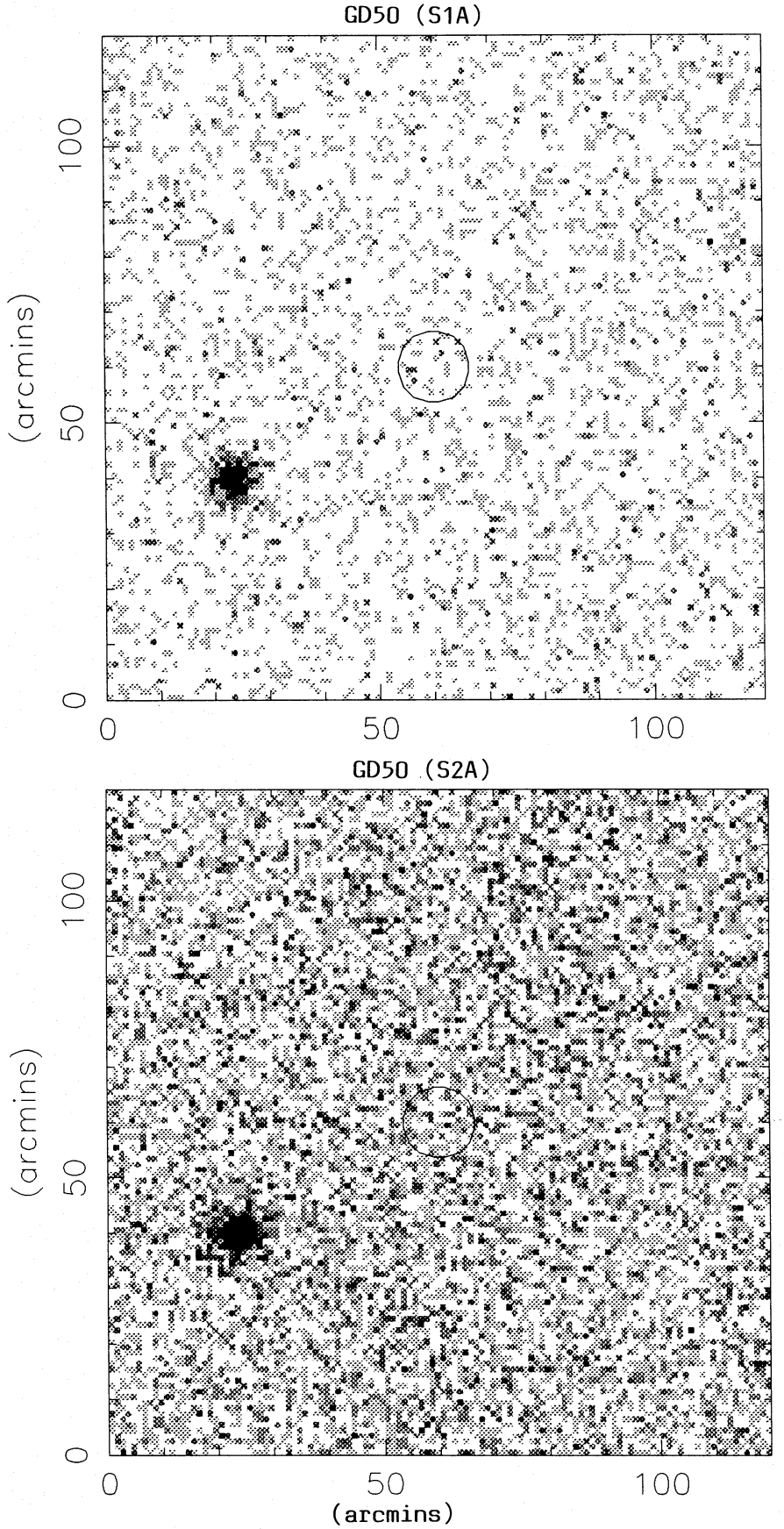

Figure 6. *ROSAT* WFC S1 and S2 images of the GD50 field, centred on the position of WD 0343 − 007 [RA (1950) = $3^h43^m53^s$, Dec. (1950) = $-00^d47'.8$], which is clearly not detected. The image is plotted in the usual celestial coordintes, with RA and Dec. along the *x*- and *y*-axes respectively (in arcmin).

represent predictions for a pure H atmosphere and an H I column of 2.5×10^{18} cm^{-2}. The predicted ratios are remarkably insensitive to temperature, varying by only 20–30 per cent between 25 000 and 60 000 K. Interstellar absorption reduces the observed ratios below the predictions, whereas photospheric opacity acts to increase them. It is interesting to note that, while the emergent fluxes of GD394 are clearly suppressed by an opacity source, the flux ratios are similar to the pure H model. It is therefore the combined information from both Figs 7 and 8 that allows us to understand each individual object.

It is clear that, except for HZ43, all objects with temperatures above 50 000 K have substantial photospheric opacity with modest H I absorption. There seems to be no clear relationship between the emergent fluxes and temperature, implying that either the nature or the abundances of the absorbers vary from star to star. HZ43 has long been considered to be the archetypal white dwarf EUV/X-ray source. At least within this sample, however, it is a unique object in having little if any photospheric opacity source in addition to H.

Turning now to those stars with temperatures between 40 000 and 50 000 K, it is clear that at least in GD2 and KUV18004 the interstellar absorption is substantial, since the S2 fluxes are lower than the S1 fluxes in both examples. Both GD257 and GD2 show about the same decrement in the PSPC flux, indicative of a similar opacity in this band. Less attenuation is seen in the S2 and S1 bands for GD257, however, suggesting a somewhat lower H I column than for GD2 and implying that some of the opacity affecting the PSPC flux is photospheric. GD984 appears to have a rather low column, and so most of the opacity seen in this star must be photospheric.

5 DISCUSSION

The results of the *ROSAT* sky survey have profound implications for our view of white dwarf composition and structure. In the detailed study of 30 previously catalogued DAs presented here we have found clear evidence that, in the hottest stars, trace photospheric opacity sources in addition to He, if indeed this element is even present, are needed to explain the data. In all, the EUV/X-ray fluxes of nine out of the 30 stars studied cannot be explained by either homogeneous or stratified H+He models. Important additional evidence for both the presence and nature of these elements can be found in high-dispersion *IUE* spectra obtained for a few of the brightest white dwarfs (e.g. Vennes, Thejll & Shipman 1991). Some of those objects that require trace metals show observable features of elements such as N, Si and Fe in their *IUE* spectra. However, the *IUE* data may not reveal all of the species responsible for the EUV/X-ray opacity, as many important transitions are not visible in the far-UV.

Looking in more detail at the temperature distribution of the white dwarf sample, it is convenient to divide the objects into two groups, with temperatures above or below 40 000 K. The majority of stars (18) are cooler than 40 000 K. Five (EG70, GD394, GD50, GD80 and V471 Tau) show evidence of photospheric heavy elements. The remainder all have EUV/X-ray fluxes that are consistent with nearly pure H atmospheres. Traces of He may be

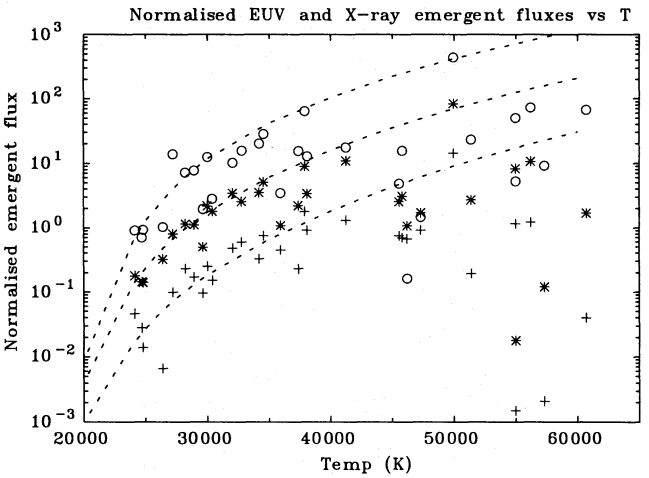

Figure 7. X-ray/EUV count rates, normalized by the *V*-magnitude instrumental effective areas and pass-bands to yield estimates of the emergent flux for each white dwarf in the survey sample. Open circles, asterisks and pluses represent the S2, S1 and PSPC values respectively. The dashed lines correspond to the predicted value for a pure H atmosphere with modest H I column (2.5×10^{18} cm^{-2}): top = S2; centre = S1; bottom = PSPC.

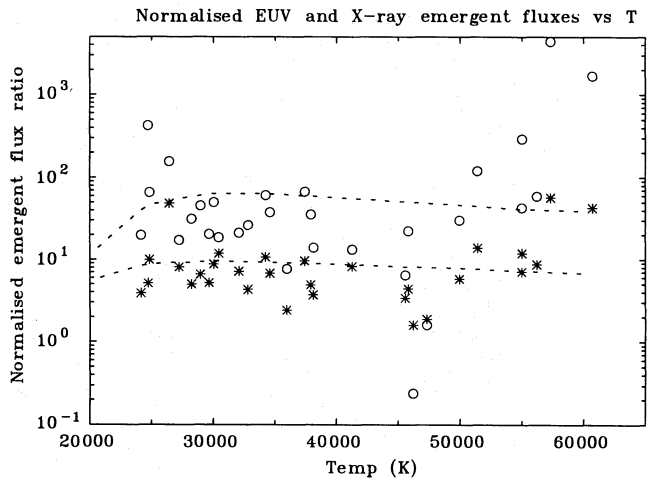

Figure 8. EUV/X-ray flux ratios for each white dwarf in the survey sample. Open circles and asterisks represent the S2:PSPC and S1:PSPC values respectively. The dashed lines correspond to the predicted values for a pure H atmosphere with modest H I column (2.5×10^{18} cm^{-2}): top = S2:PSPC; bottom = S1:PSPC.

present with an abundance of less than $\approx1\times10^{-5}$, if assumed to be homogeneously mixed. If stratified, then the implied lower limit to the H-layer mass is $\approx3\times10^{-13}M_{\odot}$. We note, however, that in general our data do not require the presence of He in any individual star. There are 12 white dwarfs in the sample with temperatures above 40 000 K, and six appear to contain the heavy-element opacity sources discussed above. Only two, PG 1123+189 and PG 1234+482, can be explained by stratified models with thinner H layers, but they could also contain metals. In GD2, GD257 and KUV18004 there is substantial interstellar opacity present, and so we cannot make unambiguous state-

ments about the presence or absence of any photospheric opacity sources. HZ43 is the only DA in this group that is clearly pure H (or nearly so), having an He abundance/H-layer mass limit similar to those of stars below 40 000 K. The very hottest DAs, above 50 000 K, show considerable dispersion in their EUV/X-ray opacities. There is no evidence for such a dispersion in the 40 000–50 000 K range but, with a small number of objects to consider, the statistical basis for any strong conclusion to be drawn is weak.

Is it possible to explain the results of this study with existing theories of the physics of white dwarf envelopes? In the past, a number of mechanisms have been invoked that might explain the presence of trace materials. Accretion from the interstellar medium or, in the case of objects like Feige 24, from the wind of a companion is one idea that has received attention. Significant progress has also been made in the study of the effect of radiative levitation of specific elements against the downward force of gravity. In the first instance, the accretion rate will be determined by the local density of interstellar material and gravity of the star. How much of the accreted matter will remain visible in the photosphere must then depend on the balance of radiative and gravitational forces. This must be a dynamic process, but if accretion is a minimal contributor, as concluded by Vennes et al. (1988), then the equilibrium of radiation pressure and gravity will determine the observed abundances. It may not be necessary to invoke either accretion or levitation if the star is stratified and has a sufficiently thin H layer, allowing us to 'see' the underlying He.

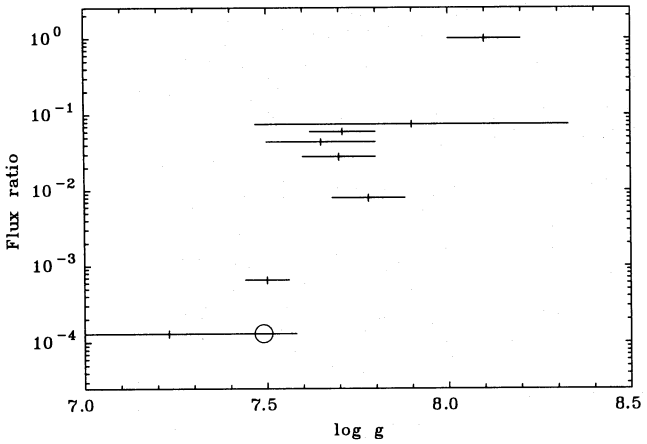

Figure 9. Ratio of the estimated emergent S1 fluxes to the values predicted for a pure H atmosphere as a function of log *g*. The sample is restricted to those white dwarfs with temperatures above 50 000 K and low H I columns.

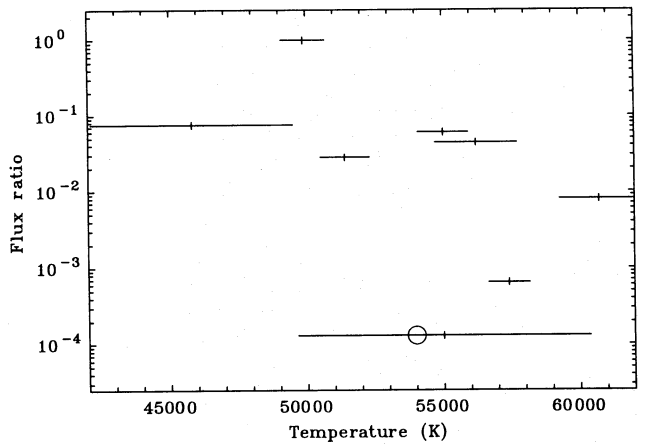

Figure 10. Ratio of the estimated emergent S1 fluxes to the values predicted for a pure H atmosphere as a function of temperature. The sample is restricted to those white dwarfs with temperatures above 50 000 K and low H I columns.

The analysis of the *ROSAT* data that we present here leads us to conclude that, for many stars, He is not the only opacity source. For stars where H + He models are able to explain the data, the implied H-layer masses are, in general, greater than $\approx 1 \times 10^{-13} M_{\odot}$. Where H + He models do not work, requiring substantial additional opacity, we are unable to say anything about the H-layer mass because appropriate models containing trace heavy elements are not available. It seems unlikely, however, that these stars are substantially different. This proposition is supported by the absence of a significant He feature at 228 Å in the spectra of Feige 24 (Paerels et al. 1986; Vennes et al. 1989) and G191–B2B (Wilkinson et al. 1992) at limits similar to those we have obtained for the cooler DAs.

As a mechanism to counteract gravitational stratification, the selective radiative levitation of elements such as C, N, O, Si and Fe is much more effective than it is for He. This is because these ions possess a larger number of strong transitions and hence higher radiative cross-sections than does He. Far-UV (e.g. Vennes et al. 1991; Tweedy 1991; Bruhweiler & Feibelmann 1993; Sion et al. 1992) and EUV spectra of the white dwarfs Feige 24 (Paerels et al. 1986; Vennes et al. 1989) and G191 − B2B (Wilkinson et al. 1992) show features resulting from these elements, although it is often difficult to demonstrate that they are definitely photospheric. Theoretical calculations by a number of groups demonstrate that radiative forces are able to support significant abundances of all these materials against gravitational settling, in the absence of any other disrupting mechanisms (e.g. accretion). Morvan et al. (1986), Vauclair (1989) and Chayer et al. (1989) have predicted the equilibrium abundances of C, N, O and Si in DA white dwarf atmospheres as a function of temperature. These independent calculations are in agreement in predicting that abundances of C, N and O increase monotonically with temperature, whereas the abundance of Si decreases above 50 000 K and is roughly constant down to 30 000 K. More recently, Chayer, Fontaine & Wesemael (1991) have also considered the radiative levitation of Fe. They found that observable abundances of Fe can only arise in DA white dwarfs at temperatures above 50 000 K, i.e. when the radiative acceleration exceeds the downward gravitational acceleration. Above this value, the Fe abundance increases towards higher temperatures.

The *ROSAT* observations fit in well with the overall picture predicted by this theory. Those DAs that show the greatest EUV/X-ray opacity effects are all hotter than 50 000 K. This would indicate that Fe is a significant contributor to the overall absorption in these stars. Radiative levitation can also explain the absence of detections for DAs hotter than 60 000 K, if the increased abundances of all species provide enough opacity to reduce the emergent EUV

and X-ray fluxes below observable limits. Since the PSPC and S1 detections of G191–B2B and Feige 24 are already close to the detection thresholds, and since WD 0343 − 007, which seems to lie in a direction of low H I column, was not detected at all, this seems to be a very plausible hypothesis. The apparent dispersion in the level of opacity, as reflected in the emergent EUV and X-ray fluxes, may be a result of differing gravities from star to star. In the absence of any other effects, radiative levitation should allow greater photospheric abundances in lower gravity stars. A survey of the various gravity determinations (e.g. K91; Vennes 1992; FKB) indicates that Feige 24 and G191–B2B have the lowest gravity, with log $g \approx 7.4$ and 7.5 respectively, and the highest degree of opacity. GD246, WD 1123 + 189 and PG 1234 + 482 all have log g of about 7.7. In contrast, the only object in which we see no opacity sources other than H, HZ43, appears to have the highest gravity. FKB obtain a value for log g in the range ≈ 7.75–8.2 from two independent measurements, and Vennes (1992) obtained a value of 8.1. We note that K91 measured log g to be 7.6, although the error of 0.34 is quite large and not necessarily inconsistent with the higher results.

To test the relationship between opacity and gravity further, we have calculated the ratio of the observed flux in the S1a filter to that predicted for a pure H atmosphere (i.e. what we would expect at the value of $T_{\rm eff}$ for any individual star in the absence of any additional opacity sources), displaying it as a function of gravity (Fig. 9). Since opacity might also depend upon $T_{\rm eff}$, these ratios are also plotted as a function of $T_{\rm eff}$ in Fig. 10. We use the S1 data here because all of the stars in question were detected in this band (cf. the non-detection of Feige 24 in the PSPC band) and the flux is less sensitive to the effects of interstellar absorption than in S2. There appears to be a correlation of this flux ratio with gravity, indicating that the photospheric opacity is highest in the lowest gravity stars. A linear fit to the observations in Fig. 9 has a correlation coefficient of 0.69, corresponding to a probability of 95 per cent that such a fit is a good description of the data. There is no particular physical reason why there should be a linear relationship between the flux ratio and gravity, and other functions may fit equally well, but the correlation test serves to illustrate the significance of the result. No similar correlation of flux with $T_{\rm eff}$ is seen in Fig. 10, suggesting that, within the small sample studied, gravity is the dominant effect. However, with such a small number of stars and the uncertainties in the determination of log g, particularly systematic errors that may vary between the samples from which we take the data, we can only say that the *ROSAT* data show possible evidence for the dependence of photospheric opacity (and, by implication, abundance) on log g and not, at the moment, conclusive proof.

If this result does stand up to closer examination, it will be an important test of radiative levitation theory. Vauclair's (1989) studies of C, N, O and Si predict that the gravity dependence of the observed abundances should be rather weak. In contrast, the abundance of Fe (Chayer et al. 1991), which may well be the most important contributor to the EUV opacity, could be critically dependent upon the balance between gravitational and radiative accelerations if the two effects are of similar magnitude.

There are two stars that show clear extra opacity in Fig. 7 at temperatures below 40 000 K: GD394 (37 000 K) and EG70 (26 400 K). The radiative levitation calculations discussed above would suggest that none of C, N, O or Fe can be responsible. Si can be present, however, in significant quantities down to $\approx 20\,000$ K. Neither star has an outstandingly lower gravity when compared with others of similar temperature. Vennes et al. (1991) reported that, in the case of GD394, the abundance determinations for Si II, Si III and Si IV show that the ionization balance does not follow the Saha–Boltzmann prescription, suggesting a non-photospheric origin. Furthermore, the velocity of the observed C, N and Si lines is some 70 km s^{-1} different from that of the Balmer lines. It may therefore be that the opacity sources are circumstellar in these cases, with their peculiarity arising from the local environment rather than from the stars themselves.

The results of this study have implications for our view of the origin and subsequent evolution of white dwarfs. Assuming that the sample of objects in this initial study (selected on the basis of the availability of temperature and log g measurements) is representative of DA white dwarfs in general, we are able to make several statements.

(i) Most DAs hotter than 50 000 K contain trace heavy elements in their atmospheres that make substantial contributions to the EUV/X-ray opacity as a result of radiative levitation, with surface gravity determining the abundances observed.

(ii) Most DAs cooler than 40 000 K contain little material in their atmospheres other than H, although we cannot rule out completely the presence of some trace He and/or heavier elements, in keeping with the diminishing effectiveness of radiative levitation as white dwarfs cool.

(iii) In general, it appears that the photospheric compositions of DA white dwarfs are dominated by the balance between gravitational settling and radiative levitation.

The importance of gravity and radiative levitation may give us clues to the relationship between the DAs, DOs and intermediate objects such as the DAOs. Radiative levitation cannot explain the extreme abundance differences found between the CO-rich PG1159 stars, which are most likely to be the result of post-AGB evolutionary processes, H-rich DOs and the DAs, but it can probably explain the traces of Fe and other elements. It seems, when we combine the results of this work with the few existing EUV spectra, that by the time stars appear as DA white dwarfs there is little or no He to be found in their photospheres. This implies that separation of H and He through gravitational settling is complete at least to the extent that the envelopes are thick enough to appear effectively as pure H (except for the trace metals that we detect). Holberg et al. (1989) have measured the abundance of He in a small sample of hot DA and DAO stars. There is no correlation of abundance with temperature and, in fact, the highest measured abundances (log He/H = − 1.0) occur in the two coolest stars observed, PG 1305 − 017 and PG 1210 + 533. Furthermore, no He is detected in four objects that all have temperatures above 60 000 K.

Vennes et al. (1988) have demonstrated that radiative levitation is unable to explain the high He abundances found by Holberg et al., and concluded that they result from thin H layers. Different He abundances then imply variations in the

H-layer mass from star to star. We must ask the question why the DAOs have layer masses, at $<2\times10^{-15}M_{\odot}$, much less than those we find to be typical of DAs in general ($>1\times10^{-13}M_{\odot}$). Studies of gravitational separation of H and He have concentrated on the downward settling of the He in a predominantly H envelope. The general approach is to consider equilibrium conditions with the H and He fully separated. Little or no detailed attention has been paid to the alternative picture of trace H in a predominantly He envelope migrating to the top of the atmosphere, although the possibility has previously been mentioned by Vennes et al. (1988). We might then explain the differences in layer masses at any particular effective temperature as a variation in the residual H remaining mixed in the photosphere at white dwarf birth. DAO objects would then be expected to join the DA sequence at a lower temperature than objects like Feige 24 and G191–B2B, and the DO–DB temperature gap would be a natural consequence of the process and would imply some lower limit to the residual H abundance. There are not yet any theoretical calculations that test this proposition. Limits placed on the residual H in progenitors such as the PG1159 stars are not restrictive enough (H/He < 1: Werner, Heber & Hunger 1991) to rule out the possibility, since at very high temperatures H is almost completely ionized and very difficult to detect. Furthermore, pulsation studies of the archetypal object PG 1159 − 035 suggest a stratified atmospheric structure including an H layer (Winget et al. 1991). If DA white dwarfs form from DOs via the DAO objects, as discussed above, where are the stars with intermediate layer masses that *ROSAT* should have been able to detect, but did not? It is likely that these objects will be rare. For the appropriate temperature range (40 000–50 000 K) within which we might expect to find them in our sample, the likelihood of finding such a star in our small sample is rather low. Also, the atmospheric composition of these stars need not be H + He alone. Some of the stars that we believe contain trace heavy elements may indeed have H-layer masses that are lower than we find in other DAs but which are only detectable with EUV spectroscopy.

The upward migration idea does cause a conflict with standard evolution theory (Iben & Tutukov 1984; Iben & MacDonald 1985; Koester & Schönberner 1986), which predicts that DA white dwarfs should be born with massive H layers ($\approx10^{-4}M_{\odot}$). However, pulsation theory demands that ZZ Ceti white dwarfs have layers of less than $10^{-8}M_{\odot}$ if the predicted blue edge of the instability strip is to match that observed ($\approx13\,000$ K, e.g. Winget et al. 1982). Further evidence against thick layers is based on the need to account for the turnover of white dwarf statistics in favour of He-dominated atmospheres at low effective temperatures. Convective mixing of a thin H layer with an underlying He convection zone is the most likely explanation, but the H mass must be less than $\approx10^{-8}M_{\odot}$ (e.g. Sion 1984). At the moment, we believe that the weight of evidence is against evolutionary theory, and that more detailed studies of H migration in He (or even C/O) atmospheres are urgently required.

6 CONCLUSION

This paper has presented the results of a detailed analysis of EUV and X-ray observations of a sample of 30 DA white dwarfs observed during the *ROSAT* sky survey and in the subsequent pointed phase of the mission. We have found that most of the hottest DA white dwarfs (>40 000 K) appear to have heavy-element opacity sources in their atmospheres, in keeping with the predictions of radiative levitation calculations. It appears that He makes a minimal contribution to the overall photospheric opacity and, as a consequence, there is a problem in linking the normal DAs to the related DOs and hybrid DAOs which have clearly visible He features. However, this difficulty could arise from the fact that the broad-band photometry available with *ROSAT* cannot necessarily separate the effects of absorption from those of trace He and trace heavy elements. This question can only be answered by spectroscopic observations in the EUV. The launch of *EUVE* in 1992 June has now given us the prospect of acquiring these spectroscopic data for a significant sample of DA white dwarfs. We look forward to these observations, which will also test further the conclusions drawn and predictions made here.

ACKNOWLEDGMENTS

The *ROSAT* project is a joint Germany/UK/USA project supported by BMFT (Germany), SERC (UK) and NASA. We are grateful to the large number of scientists involved in building and operating the satellite, without whom this work would have been impossible. *ROSAT* data analysis was performed on the Leicester and Birmingham nodes of the Starlink computer network, which is also funded by SERC. MAB is funded through an SERC Advanced Fellowship, AES and SSR by SERC PDRA posts, and CJD and MCM by SERC Research Studentships. DK, DSF, JBH and KK are all supported by a combination of NASA and NSF grants.

REFERENCES

Barstow M. A., 1989, in Wegner G., ed., White Dwarfs. Springer-Verlag, Berlin, p. 156
Barstow M. A., 1990, MNRAS, 243, 182
Barstow M. A., Schmitt J. H. M. M., Clemens J. C., Pye J. P., Denby M., Harris A. W., Pankiewicz G. S., 1992, MNRAS, 255, 369
Barstow M. A., Fleming T. A., Finley D. S., Koester D., Diamond C. J., 1993a, MNRAS, 260, 631
Barstow M. A. et al., 1993b, MNRAS, submitted
Bergeron P., Saffer R. A., Liebert J., 1992, ApJ, 394, 228
Bruhweiler F. C., Feibelman 1993, AJ, 105, 1477
Chayer P., Fontaine G., Wesemael F., 1989, in Wegner G., ed., White Dwarfs. Springer-Verlag, Berlin, p. 253
Chayer P., Fontaine G., Wesemael F., 1991, in Vauclair G., Sion E., eds, White Dwarfs. Kluwer, Dordrecht, p. 249
Fleming T. A., Liebert J., Green R. G., 1986, ApJ, 308, 176
Fleming T. A., Barstow M. A., Sansom A. E., Holberg J. B., Liebert J., Tweedy R., 1993, in Barstow M. A., ed., White Dwarfs: Advances in Observation and Theory. Kluwer, Dordrecht, in press
Frisch P. C., York D. G., 1983, ApJ, 271, L59
Holberg J. B., Kidder K., Liebert J., Wesemael F., 1989, in Wegner G., ed., White Dwarfs. Springer-Verlag, Berlin, p. 188
Hubeny I., 1988, Comput. Phys. Commun., 52, 103
Iben I., Jr, Macdonald J., 1985, ApJ, 296, 540
Iben I., Jr, Tutukov A. V., 1984, ApJ, 282, 615
Kidder K. M., 1991, PhD thesis, University of Arizona (K91)
Kidder K. M., Holberg J. B., Barstow M. A., Tweedy R. W., Wesemael F., 1992, ApJ, 394, 288
Koester D., 1989, ApJ, 342, 999

Koester D., 1991, in Michaud G., Tutukov A., eds, Proc. IAU Symp. 145, Evolution of Stars: The Photospheric Abundance Connection. Kluwer, Dordrecht, p. 435
Koester D., Schönberner D., 1986, A&A, 154, 125
Morvan E., Vauclair G., Vauclair S., 1986, A&A, 163, 145
Paerels F. B. S., Heise J., 1989, ApJ, 339, 1000
Paerels F. B. S., Bleeker J. A. M., Brinkman A. C., Heise J., 1986, ApJ, 309, L33
Pfefferman E. et al., 1986, Proc. SPIE, 733, 519
Pounds K. A. et al., 1993, MNRAS, 260, 77
Reid N., Wegner G., 1988, ApJ, 335, 953
Saxton R. D., 1991, Starlink User Note 98, Starlink Software Collection
Sion E. M., 1984, ApJ, 282, 612
Sion E. M., 1986, PASP, 98, 821
Sion E. M., Bohlin R. C., Tweedy R. W., Vauclair G. P., 1992, ApJ, 391, L29
Tweedy R. W., 1991, PhD thesis, University of Leicester
Vauclair G., 1989, in Wegner G., ed., White Dwarfs. Springer-Verlag, Berlin, p. 176
Vennes S., 1992, ApJ, 390, 590
Vennes S., Pelletier C., Fontaine G., Wesemael F., 1988, ApJ, 331, 876
Vennes S., Chayer P., Fontaine G., Wesemael F., 1989, in Wegner G., ed., White Dwarfs. Springer-Verlag, Berlin, p. 373
Vennes S., Thejll P., Shipman H. L., 1991, in Vauclair G., Sion E., eds, White Dwarfs. Kluwer, Dordrecht, p. 235
Wegner G., McMahon R. K., Boley F. I., 1987, AJ, 94, 1271
Weidemann V., 1990, ARA&A, 28, 103
Wells A. et al., 1990, Proc. SPIE, 1344, 230
Werner K., Heber U., Hunger K., 1991, A&A, 244, 437
Wesemael F., Auer L. H., Van Horn H. M., Savedoff M. P., 1980, ApJS, 43, 159
Wilkinson E., Green J. C., Cash W., 1992, ApJ, 397, L51
Winget D. E., Van Horn H. M., Tassoul M., Hansen C. J., Fontaine G., Carroll B. W., 1982, ApJ, 253, L29
Winget D. E. et al., 1991, ApJ, 378, 326